

## Structure development in $\text{Co}_{38}\text{Ni}_{33}\text{Al}_{29}$ ferromagnetic shape memory alloy

Jaromír Kopeček<sup>a</sup>, Silvie Sedláková-Ignáčová, Karel Jurek, Markéta Jarošová, Jan Drahekoupil, Petr Šittner, Václav Novák

Institute of Physics AS CR, v.v.i., 182 21 Praha, Czech Republic

**Abstract.** In the present study, a set of the directionally solidified samples from ferromagnetic shape memory alloy with the nominal composition  $\text{Co}_{38}\text{Ni}_{33}\text{Al}_{29}$  was prepared using the Bridgman method. It is shown that various growth rates result in various solidification structures of the crystals, mainly in different ratios of the disordered phase  $\gamma$  - cobalt solid solution and the ordered phase  $\beta$  - B2 (Co,Ni)Al. This ratio has the fundamental effect on the temperature of the martensitic phase transition. The results are compared with the structure of samples prepared by the floating zone method. The structures of samples prepared with the different growth rate were studied by metallography, SEM, EDX, and EBSD methods. The samples without high-angle grain boundaries were cut from the prepared crystals for the mechanical testing.

### 1. Introduction

Ferromagnetic shape memory alloys (FSMA) are interesting and frequently investigated materials, which attract attention by the interaction between ferromagnetic and martensitic domains. There can be generally two kinds of such interaction: magnetically induced martensite reorientation - in the case, when the magnetic field leads to the reorientation of the structural martensitic domain, and magnetically induced martensite transformation, when magnetic field even causes martensitic transformation [1]. Both these effects are observed and exploited in Ni-Mn-Ga alloys [2,3]. Unfortunately, these alloys have some metallurgical obstacles for practical use like poor room temperature ductility or low fatigue resistance. One class of materials, where better mechanical properties are expected, is based on the system Co-Ni-Al [4-6].

The shape memory effect is strongly affected by the high-temperature state of the material, its grain structure and thermomechanical history of the sample generally. Moreover, the study of the transformation or reorientation process at the level of the interfaces requests preparation of the single-crystal samples [7]. Thus the particular focus should be given to the preparation of such samples. The Co-Ni-Al alloys as FSMA have two-phase structure [8]. The matrix of the alloy is formed by the ordered B2 or  $\beta$ -phase (Co,Ni)Al (space group Pm3m). The precipitates of the face centred cubic (fcc) cobalt solid solution marked A1 or  $\gamma$ -phase (space group Fm3m) are spread in the matrix. They originate from the interdendritic melt and can have complicated, eutectic structure with inclusion of B2 phase. The precipitates of the ordered  $L1_2$  or  $\gamma'$ -phase were observed depending on the cooling rate of the alloy. The content of particular phases depends on the composition and condition of preparation [9].

The ordered B2 phase undergoes martensitic transformation into the tetragonal  $L1_0$  phase (phase group P4/mmm). The transformation mechanism is going through precursors, tweed structure and softening of phonon modes as in the Ni-Al alloys [10]. The role of the interdendritic  $\gamma$ -phase precipitates is unclear. They can trap the martensite up to higher temperature in a special configuration, but they did not stop transformation interface [6]. Various precipitates created during aging in the matrix including face centred cubic (fcc) and hexagonal close packed (hcp) cobalt,  $(\text{Co,Ni})_3\text{Al}$ , and others were observed [6,11,12].

In this work set of unidirectionally crystallized samples was prepared using Bridgman method. The original aim was to prepare transformable samples which can be used for the martensite single-crystal preparation via repeated deformation [7]. But the complex nature of the solidified samples led to the study of "as-cast" structures. Mainly, the effect of the growth rate on the presence and distribution of the phases was investigated.

---

<sup>a</sup> e-mail: kopecek@fzu.cz

## 2. Experimental procedure

The material with the composition Co - 33 at.% Ni - 29 at.% Al was remelted in the induction furnace Balzers VSG-02 and cast into rods with the diameter of the 12 mm and the length of approx. 100 mm. The single-crystals were grown from the re-cast rods using Bridgman furnace GRANAT-74. The growth process was performed in the protective argon atmosphere in the alumina conical crucibles. Bridgman crystals have diameter of 20 mm and length approximately of 70 mm. The samples for mechanical testing were spark cut, polished, annealed at 1280 °C for 4 h in argon atmosphere and quenched into the cold water. The metallography samples were spark cut and polished using conventional sequence of abrasive papers and pastes. The final step of the surface preparation was polishing with colloidal silica (OP-S).

The optical microscope Zeiss ZM1 was used for the light microscopy. The samples were characterized by scanning electron microscope JXA-733 equipped with the EDX and EBSD detectors produced by AMETEK EDAX-TSL Inc. All EDX analyses were standardized using the pure elements.

## 3. Results

The sample grown with the growth rate of  $17 \text{ mm}\cdot\text{h}^{-1}$  separates into the three-phase mantle and one-phase core, Fig. 1. The core contains just B2-phase matrix. The mantle contains B2 matrix of the same composition as in the core and precipitates of the disordered  $\gamma$ -phase (fcc cobalt solid solution) and small precipitates of the ordered  $\gamma'$ -phase ( $L1_2$  structure  $(\text{Co,Ni})_3\text{Al}$ ). The last mentioned structure is deduced from the morphology, the same precipitates in our samples were distinguished to be ordered  $\gamma'$ -phase by TEM [11]. The  $\gamma$ -phase have morphology of the interdendritic surrounded melt, which solidified at the eutectic composition. This is visible from the lamellar morphology of the bigger  $\gamma$ -phase precipitates, Fig. 1. The thickness of the mantle is approximately 40% of the sample diameter. The sample contains shrink holes and some grain boundaries. It means, the sample is not single-crystal, but the grains have similar growth direction close to the  $\langle 100 \rangle$  direction. The cracks observed in the core can be a consequence of the diamond saw cutting during metallography preparation or they can result from the solidification stresses. The cracks confirm extreme brittleness of B2 phase, as is known for decades [13].

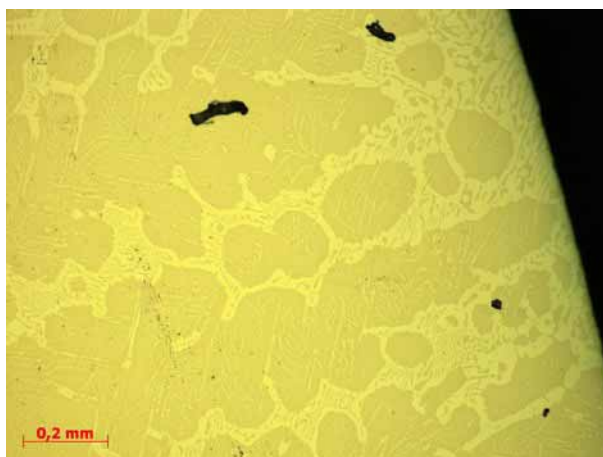


**Fig. 1** Optical metallography in the Nomarski contrast. The mantle of the sample solidified with the growth rate of  $17 \text{ mm}\cdot\text{h}^{-1}$ . Large precipitates with complicated structure have the  $\gamma$ -phase structure, while the small precipitates in between belong to the  $\gamma'$  structure. The black spots are shrink holes.

The sample grown with the growth rate of  $28 \text{ mm}\cdot\text{h}^{-1}$  has two-phase structure with the grain big enough to prepare single-crystalline cuboidal samples for the mechanical testing. This sample transforms to the martensite and shows repeatable stress induced martensitic transition with quite unusual stress-strain dependence; the mechanical testing results will be published separately [14]. Figs. 2 and 3 show metallography of two samples for the mechanical testing; the sample at Fig. 2 transforms repeatedly, the sample at Fig. 3 does not, although retained martensitic lamellas are visible between the  $\gamma$ -phase precipitates.

The sample grown with the growth rate of  $38 \text{ mm}\cdot\text{h}^{-1}$  contains three phases and the distribution of precipitates is much better than in the previous case. The interdendritic  $\gamma$ -phase precipitates and small precipitates of the  $\gamma'$ -phase embedded in the B2 matrix are presented. While the composition of the B2-phase is not changing,

there is some inhomogeneity in the amount of the  $\gamma$ -phase along the growth direction of the sample. The tip of the sample is depleted of the  $\gamma$ -phase and the middle part of it has the highest ratio of it, Fig. 4. Very high content of the  $\gamma$ -phase harms the single-crystal nature of the sample, too, after reaching some critical ratio the high-angle grain boundaries appeared.

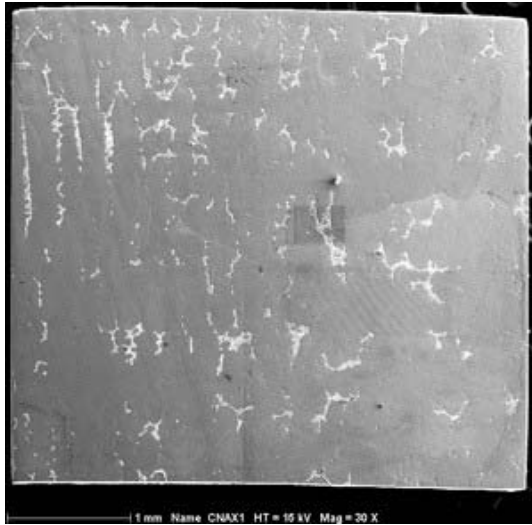


**Fig. 2** Secondary electron image from SEM of the sample grown with the growth rate of the  $28 \text{ mm}\cdot\text{h}^{-1}$ . The bright precipitates correspond to  $\gamma$ -phase.

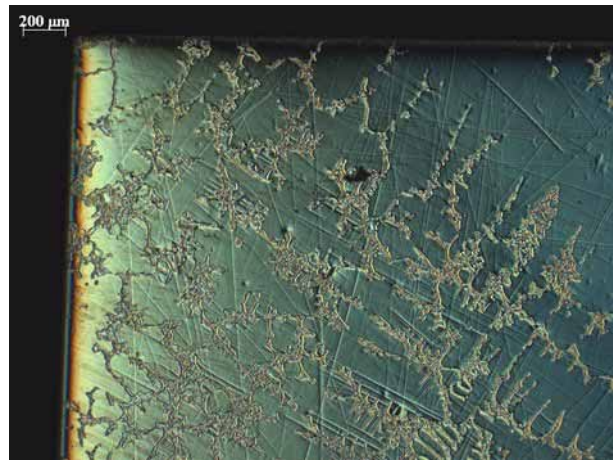
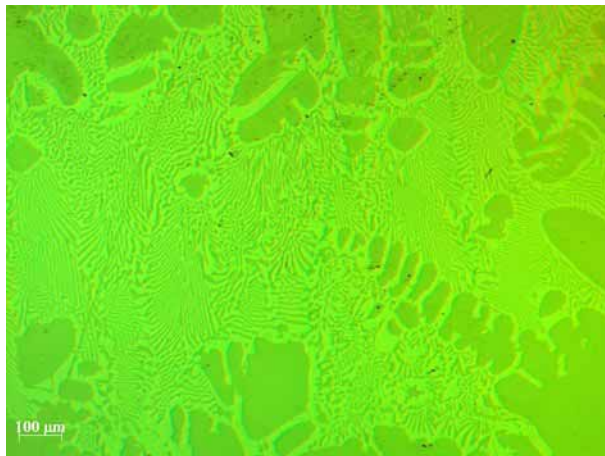
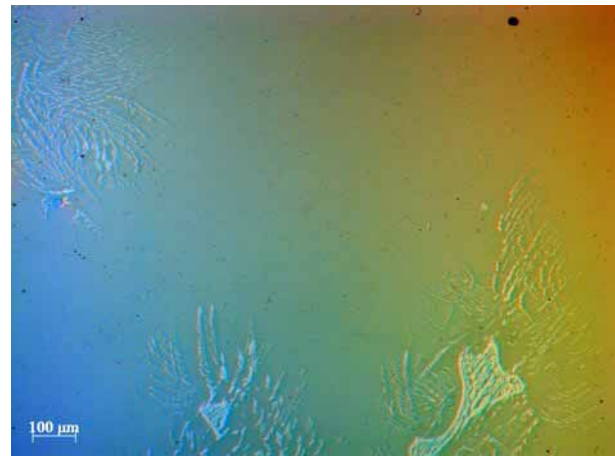


**Fig. 3** Optical metallography in the Nomarski contrast of the sample grown with the growth rate of  $28 \text{ mm}\cdot\text{h}^{-1}$ . A different piece of the same sample as in previous figure.



(a)



(b)

**Fig. 4** Optical metallography in the Nomarski contrast of the sample solidified with the growth rate of  $38 \text{ mm}\cdot\text{h}^{-1}$ . (a) middle part of the sample with the highest  $\gamma$ -phase concentration ; (b) the beginning of the sample with the lowest precipitates concentration here presented mainly by the chains of  $\gamma'$ -precipitates surrounding  $\gamma$ -phase.

The sample grown with the growth rate of  $104 \text{ mm}\cdot\text{h}^{-1}$  have homogeneous distribution of the  $\gamma$ -phase along the growth direction of the sample and as well the distribution of the elements is homogeneous. There are more grains grown in the sample compare to the previous case, but it is still possible to cut cuboidal sample. The growth direction of the sample is close to the  $\langle 100 \rangle$  direction as in the previous cases. In the case of so quickly solidified samples no one  $\gamma'$ -phase precipitates were observed.

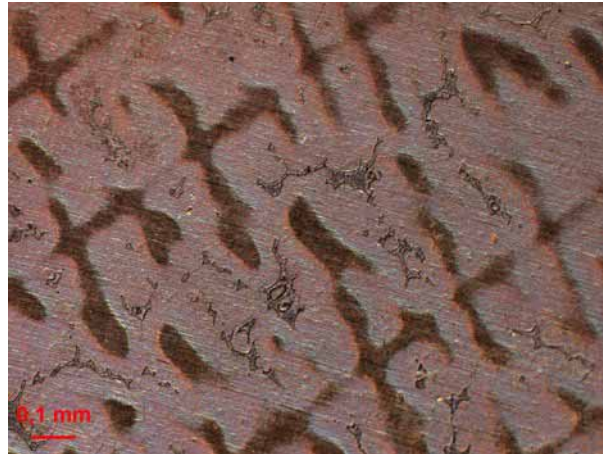


**Fig. 5** Optical metallography in the Nomarski contrast of the sample solidified with the growth rate of  $107 \text{ mm}\cdot\text{h}^{-1}$ . The  $\gamma$ -phase precipitates are visible in the bright matrix, the dark crosses represent the cores of the dendrites. The visualisation of them is a consequence of the surface chemical etching.

#### 4. Discussion

Various microstructures were found in the samples solidified with the changing growth rate, which is not any surprise. It must be noted that we do not observe equilibrium structures, at least at higher growth rates. The ternary phase diagram [8] shows enlarging ternary area of the B2,  $\gamma$  and  $\gamma'$ -phases with decreasing temperature. Thus, we can describe the presence of  $\gamma'$ -phase as the sign of equilibrium state of the alloy. The  $\gamma'$ -phase is not observed in the quickest grown sample.

**Table 1** The composition of the B2 matrix and  $\gamma$ -phase precipitates in the prepared samples. The presented errors are just the statistical standard deviations and do not contain methodological and apparatus errors.

Sample	Growth rate [ $\text{mm}\cdot\text{h}^{-1}$ ]	Composition [at. %] B2 matrix			Composition [at. %] $\gamma$ -precipitates		
		Al	Co	Ni	Al	Co	Ni
Bg179	17	$28,5 \pm 0,4$	$38,3 \pm 0,6$	$32,2 \pm 0,2$	$15,6 \pm 0,2$	$54,4 \pm 0,3$	$30,0 \pm 0,2$
BM1-CNAX1	28	$30,9 \pm 0,2$	$37,0 \pm 0,1$	$32,2 \pm 0,2$	$17,9 \pm 0,5$	$52,3 \pm 0,5$	$29,9 \pm 0,2$
BM1-CNAX2		$30,4 \pm 0,2$	$37,6 \pm 0,3$	$32,0 \pm 0,2$	$18 \pm 1$	$53 \pm 1$	$29 \pm 1$
Bg174	38	$30 \pm 2$	$37 \pm 2$	$32,6 \pm 0,6$	$16 \pm 2$	$54 \pm 3$	$29 \pm 1$
Bg190	104	$30,5 \pm 0,5$	$37,8 \pm 0,5$	$31,6 \pm 0,3$	$17 \pm 1$	$53 \pm 0,8$	$29,5 \pm 0,5$
N23	10	$31,7 \pm 0,9$	$36 \pm 1$	$32,0 \pm 0,5$	$18 \pm 4$	$53 \pm 5$	$29 \pm 1$

Table 1 summarizes the compositions of the B2 matrix and  $\gamma$ -phase precipitates in all prepared crystals. The  $\gamma'$ -phase is too small to be evaluated by available tools. It is visible that fraction of nickel is de-facto constant in respective phases. What vary significantly is fraction of cobalt and aluminum. We can recognize quite different grouping of the data than from the point of the  $\gamma'$ -phase. The occupation of aluminum in the B2 matrix is around 28 at.% just for crystal grown with the growth rate of  $17 \text{ mm}\cdot\text{h}^{-1}$ . For the higher growth rates the aluminum concentration in the B2 phase varies around or above 30 at.%. The cobalt concentration behaves in the opposite way.

The last line in Table 1 shows the results from the floating zone method prepared crystal. Those results are in detail described in Ref. 15. The morphology of the floating zone crystal grown with growth rate of  $10 \text{ mm}\cdot\text{h}^{-1}$  and Bridgman crystal grown with growth rate of  $17 \text{ mm}\cdot\text{h}^{-1}$  is similar, both split into the mantle and core. In accordance with the nature of the thermal field in both methods we can see that thermal gradient in Bridgman furnace is smoother. The  $\gamma'$ -phase appears and the concentration of aluminum in the B2 matrix is the lowest from all studied samples. In the floating zone sample with the similar growth rate the  $\gamma'$ -phase did not appear and the concentration of aluminum is even higher than in the Bridgman samples solidified with the growth rate of  $107 \text{ mm}\cdot\text{h}^{-1}$ .

Here we can mention as well that enhancement of the crystals' mantle with cobalt in the floating-zone sample is caused by the effect of centrifugal force. The Bridgman sample grown with the growth rate of  $17 \text{ mm}\cdot\text{h}^{-1}$  did not show the enhancement by cobalt close to the surface.

It is obvious from the discussed data that the main varying variable is the ratio of  $\gamma$ -phase (and eventually  $\gamma'$ -phase) to B2 phase. The material behaves in agreement with the ternary phase diagram - excess cobalt solidifies in the form of  $\gamma$ -phase. The transformation temperature is established by the high-temperature annealing followed by quenching. During this process the  $\gamma'$ -phase precipitates are usually melted, sometimes even the  $\gamma$ -phase precipitates. In spite of the dissolving of the precipitates, their original distribution and ratio of the precipitates to matrix are the main factors influencing the final transformational temperature in the nonequilibrium samples.

## 5. Conclusions

Samples of ferromagnetic shape memory alloy  $\text{Co}_{38}\text{Ni}_{33}\text{Al}_{29}$  were unidirectionally crystallized by the Bridgman method using various growth rates. The dependence of microstructures on the used growth rate was investigated. The dendritic growth was observed for any growth rate. It was shown that the structure formation is controlled by the thermodynamic and kinetic parameters of the solidification process. Three phase structures of B2,  $\gamma$  and  $\gamma'$  are stable up to the growth rate of  $38 \text{ mm}\cdot\text{h}^{-1}$ . A change of the composition of the B2 matrix and  $\gamma$ -phase precipitates was observed between the growth rates of  $17 \text{ mm}\cdot\text{h}^{-1}$  and  $28 \text{ mm}\cdot\text{h}^{-1}$ . The higher growth rate the higher amount of the grain boundaries; the lower growth rate the higher spatial nonuniformity of the  $\gamma$ -phase. The ratio of the B2 and  $\gamma$ -phase existing in the sample affects its mechanical properties, particularly the martensite transformation temperature and through it the transformation stress for the stress induced martensitic transformation.

### Acknowledgement

Authors would like to acknowledge the financial support from the Grant Agency of the AS CR No. A200100627, IAA200100902 and Czech Science Foundation No. 101/09/0702.

### References

- [1] R.C. O'Handley, *J. Appl. Phys.* **83**, 3263 (1998)
- [2] O. Heczko, A. Sozinov, K. Ullakko, *IEEE Trans. Magn.* **36**, 3266 (2000)
- [3] F. Khelifaoui, M. Kohl, J. Buschbeck, O. Heczko, S. Fähler, L. Schultz, *Eur. Phys. J Special Topics* **158**, 167 (2008)
- [4] K. Oikawa, L. Wulff, T. Iijima, F. Gejima, T. Ohmori, A. Fujita, K. Fukamichi, R. Kainuma and K. Ishida, *Appl. Phys. Lett.* **79**, 3290 (2001)
- [5] R. Kainuma, M. Ise, C. C. Jia, H. Ohtani, K. Ishida, *Intermetallics* **4**, S151 (1996)
- [6] Yu. I. Chumlyakov, I. V. Kireeva, E. Yu. Panchenko, E. E. Timofeeva, Z. V. Pobedennaya, S. V. Chusov, I. Karaman, H. Maier, E. Cesari and V. A. Kirillov, *Russ. Phys. J.* **51**, 1016 (2008)
- [7] V. Novak, P. Sittner, S. Ignacova, T. Cernoch, *Mater. Sci. Engn. A* **438-440**, 755 (2006)
- [8] M.H. Protopopescu, H. Hubert in P. Günter, G. Effenberg, *Ternary alloys, Vol. 4 Al-Cd-Ce to Al-Cu-Ru* (VCH, Weinheim, 1991), p. 234
- [9] J. Liu, H.X. Zheng, Y. Huang, M. Xia, J.G. Li, *Scr. Mater.* **53**, 29 (2005)
- [10] Y. Murakami, D. Shindo, K. Oikawa, R. Kainuma, K. Ishida, *Acta Mater.* **50**, 2173 (2002)
- [11] B. Bartova, D. Schryvers, Z. Q. Yang, S. Ignacova, P. Sittner, *Scripta Mater.* **57**, 37 (2007)
- [12] B. Bartova, N. Wiese, D. Schryvers, N. J. Chapman, S. Ignacova, *Acta Mater.* **56**, 4470 (2008)
- [13] L. A. Hocking, *J. Inst. Met.*, **99**, 98 (1971)
- [14] S. Sedlakova-Ignacova, J. Kopecek, P. Sittner, V. Novak, unpublished results
- [15] J. Kopeček, K. Jurek, M. Jarošová, J. Drahoukoupil, S. Sedláková-Ignáčová, P. Šittner, V. Novák, *Proc. EMAS 2009*, in press